AIAA SciTech 2020 AIAA-2020-0685
6 - 10 Jan 2020, Orlando, FL

Wake Response Downstream of a Spanwise-Oscillating Hemispherical Turret

Aaron Roeder[1], Stanislav Gordeyev[2]
University of Notre Dame, Notre Dame, IN, 46556

and

Donald J. Wittich[3]
Air Force Research Laboratory, Directed Energy Directorate, Kirtland AFB, NM 87117

The experimental studies of the wake response downstream of an oscillating hemispherical turret at subsonic speeds are presented. The oscillating turret consists of a turret shell, mounted on an aluminum rectangular plate. The turret assembly was designed for the turret to oscillate in the spanwise direction at a single frequency, coinciding with the main frequency of the dominant wake mode. The resonant-based aero-elastic response from the flow results in the forced turret oscillations in the spanwise direction. Multiple accelerometers mounted at different points at the turret assembly were used to measure local displacements. It was demonstrated that the turret oscillates at a fixed frequency over a range of Mach numbers between 0.3 and 0.55, with the oscillation amplitude of about a millimeter. Several unsteady pressure sensors, placed on the tunnel wall downstream of the turret, were used to investigate the wake response to the oscillating turret. It was found that the pressure fluctuations are less energetic for the oscillating turret and the wake was more organized in the spanwise direction, compared to the wake downstream of the stationary turret.

I. Introduction

Turrets are currently a geometry of choice when a laser beam needs to track a target. However, when a turret-based system is placed on an aircraft, moving at transonic speeds or faster, the turbulent flow around the turret, especially the turbulent wake creates significant density variations and the corresponding aero-optical effects. These effects distort the outgoing beam by defocusing it and imposing jitter on it, which adversely affect point-and-track performance of the system. In addition, unsteady forces acting on the turret might excite unwanted mechanical vibrations inside the turret's optical layout, affecting the beam control and stabilization.

To address this issue, many studies were conducted to quantify the aero-optical [1-5] and fluidic [6-11] performance of the turrets. Unsteady spatially-resolved pressure fields on and around the turrets, obtained using pressure sensitive paint, were used to study the dynamics of the wake at various subsonic and transonic speeds [12-15]. Using pressure data, unsteady forces acting on

[1] Graduate student, Department of Aerospace and Mech. Eng AIAA Student member.
[2] Associate Professor, Department of Aerospace and Mech. Eng., AIAA Associate Fellow
[3] Aerospace Engineer, Laser Division, 3550 Aberdeen Ave SE, AIAA Senior Member

the turret were directly calculated and shown to be dominated by low-frequency, large-scale structures in the wake [16].

As it was demonstrated in several papers [14,15], proper orthogonal decomposition and a conditional analysis of the pressure field around and downstream of the turret had revealed that the main dynamic mode in the wake behind the hemispherical turret is a so-called shifting wake mode, shown in Figure 1, left. The corresponding spectral analysis of the temporal evolution of the shifting mode found that the main frequency of the mode is within the normalized frequency range $St_D = fD/U_\infty = 0.1$-0.15, as shown in Figure 1, right.

For all the mentioned studies, the turret was either rigidly mounted to the wall or assumed to be rigid in numerical studies. In real applications, however, the turret skin is relatively thin to make the turret assembly lighter. Unsteady pressure fields, especially the dominant shifting mode and a corresponding unsteady force might result in elastic deformation of the turret surface or a mechanical motion of the turret as a whole, if the mounting mechanism is not stiff enough. This aero-elastic effect potentially can cause changes in the wake dynamics and consequently modify the resulted aero-optical effects and the unsteady forces acting on the turret.

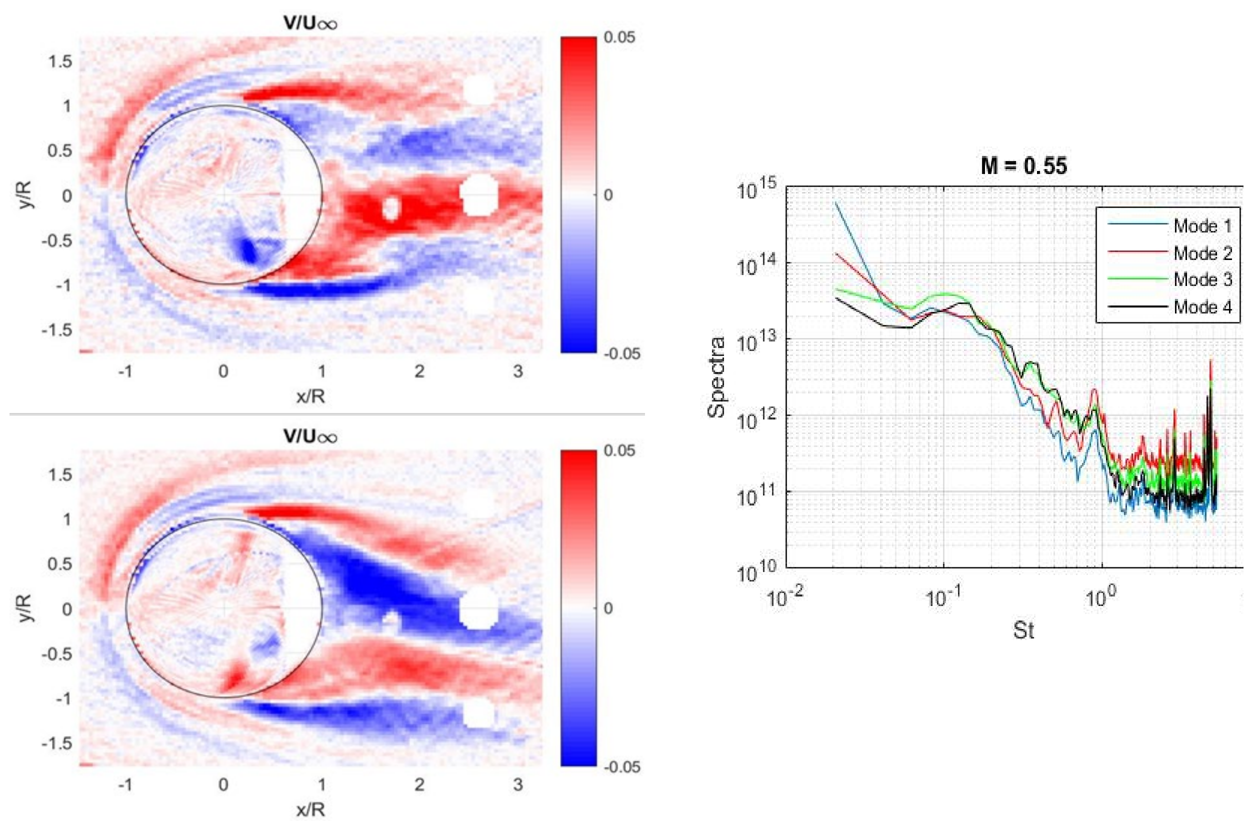

Figure 1: Left: Conditionally-averaged velocity field around the turret, from [15]. Right: spectra of dominant POD modes of the unsteady pressure field around the turret, from [14].

In the presented studies, the turret was allowed to move in the spanwise direction by placing it on a flexible plate. Parameters of the plate were chosen in such a way that the main oscillating frequency of the plate coincided with the dominant frequency of the unsteady spanwise forcing imposed on the turret. It allowed amplifying the periodic motion of the plate, resulting in the turret oscillating at a single frequency with a spanwise amplitude in an order of a millimeter. The wake response downstream of the oscillating turret is studied and compared with the wake dynamics downstream of the rigidly-mounted or stationary turret.

II. Experimental Studies

A concept of an oscillating turret, when a rigid hemispherical turret is mounted on a thin, wide rectangular aluminum plate, is schematically shown in Figure 2. The plate is aligned along the streamwise direction, so the turret can only move in the spanwise direction. In this investigation transverse oscillating cantilevered uniform Euler-Bernoulli beam theory for a beam with tip mass attachment was used to model, design, and construct an oscillating turret system and is fully described in [17]. The Euler-Bernoulli cantilever bar dynamic equations were used to demonstrate that the plate and turret system behaves as a pendulum and has a dominant oscillating frequency; this frequency depends on the elastic properties of the plate, mechanical dimensions of the plate, and the mass and the inertia of the turret. The vibrational characteristics of this system are governed by the following differential equation (1), with friction ignored:

$$E \cdot I \frac{\partial^4 w(y,t)}{\partial y^4} + m \frac{\partial^2 w(y,t)}{\partial t^2} = 0 \tag{1}$$

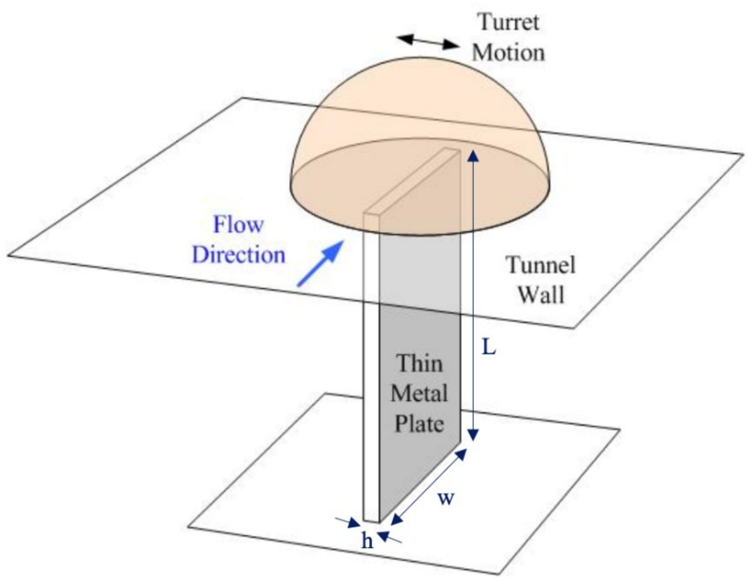

Figure 2: Schematic of the spanwise oscillating turret. Plate parameters and the system od coordinate is also indicated.

The clamped-free boundary conditions for this system are given by equations (2-5):

$$\left[E \cdot I \frac{\partial^2 w(y,t)}{\partial y^2} + I_t \frac{\partial^3 w(y,t)}{\partial t^2 \partial y}\right]_{y=L} = 0 \tag{2}$$

$$\left[E \cdot I \frac{\partial^3 w(y,t)}{\partial y^3} + M_t \frac{\partial^2 w(y,t)}{\partial t^2}\right]_{y=L} = 0 \tag{3}$$

$$w(0,t) = 0 \tag{4}$$

$$\left.\frac{\partial w(y,t)}{\partial y}\right|_{y=0} = 0 \tag{5}$$

In this model, $w(y,t)$ describes the transverse displacement of the plate in z-direction due to bending motion, where E is Young's modulus for aluminum and I is the moment of inertia of the cross-sectional area of the plate, as described by equation (6). L is the length of the plate, b is the plate width, h is the plate thickness, as schematically shown in Figure 2, $m = \rho bh$ is the plate mass per unit length of the beam and ρ is the density of the aluminum plate. M_t is the tip mass attached to the beam, which is comprised of a thin plastic turret shell and a 3 mm thick aluminum mounting disk. I_t is the moment of inertia of the tip mass about $y = L$, given by equation (7), where M_{disk} is the mass of the aluminum mounting disk, M_{turret} is the mass of the turret shell, and R is the turret/plate radius,

$$I = \frac{bh^3}{12} \tag{6}$$

$$I_t = \frac{1}{4} M_{disk} R^2 + \frac{1}{3} M_{turret} R^2 \tag{7}$$

Equations (1-5) were solved using separation of variables [17] resulting in a differential eigenvalue problem, with a characteristic equation given by equation (8).

$$1 + \cos(\lambda)\cosh(\lambda) + \lambda \frac{M_t}{mL}(\cos(\lambda)\sinh(\lambda) - \sin(\lambda)\cosh(\lambda)) - \frac{\lambda^3 I_t}{mL^3}(\cosh(\lambda)\sin(\lambda) - \sinh(\lambda)\cos(\lambda)) + \frac{\lambda^4 M_t I_t}{m^2 L^4}(1 - \cos(\lambda)\cosh(\lambda)) = 0 \tag{8}$$

The first eigenvalue, λ_1, of this characteristic equation was used to compute the undamped natural frequency of the first harmonic, f_1, using equation (8),

$$f_1 = \frac{\lambda_1^2}{2\pi}\sqrt{\frac{E \cdot I}{mL^4}} \tag{8}$$

Equations (8-9) were used to compute relationship between the resonant frequency of the oscillating turret system, as a function of plate length, L, and the plate thickness, h. For the presented studies, the turret diameter was chosen to be D = 10" and the freestream Mach number to be between M = 0.3 and 0.55. For these parameters, $St_D = 0.15$ corresponds to a range of frequencies between 80 and 100 Hz, so the target oscillating frequency of the system was chosen to be 90 Hz. The plate material was 2014-series aluminum alloy, which was chosen for its fatigue-resistant properties. All relevant parameters of the turret and the plate used to compute the resonant frequency are presented in Table 1. Figure 3 shows a contour plot of the oscillating frequencies for different plate thickness and lengths. The red curve in Figure 3 describes the desired frequency of 90 Hz. Based on this plot, the thickness of the aluminum plate was chosen to be h = 12.7 mm and the plate length was chosen to L = 230 mm.

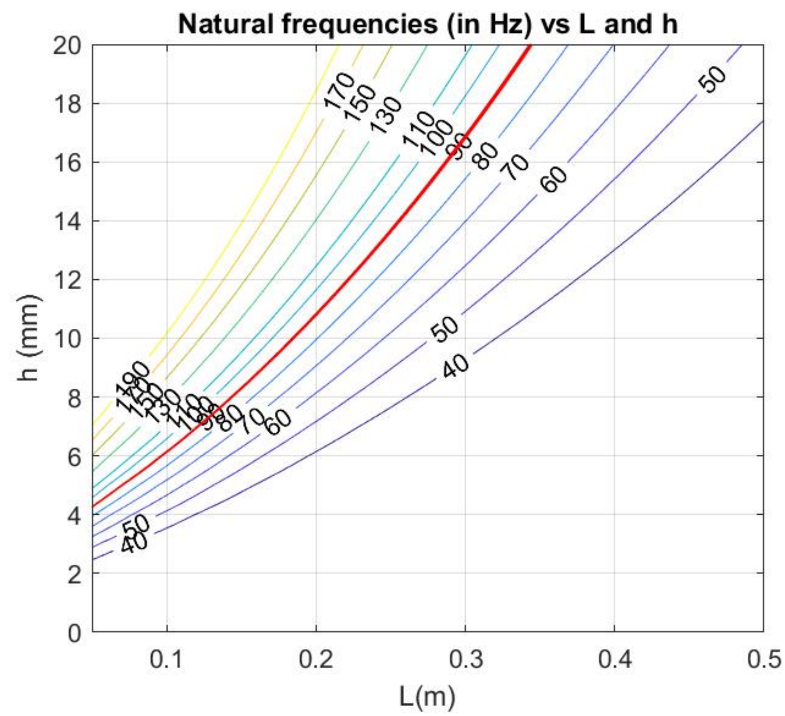

Figure 3: Natural frequency of free oscillations for the 1st vibrational mode of the turret system as a function of plate length, L, and thickness, h. The target frequency of 90 Hz is indicated by thick red line.

Table 1: Parameters of the oscillating turret system

Plate Thickness, h	Plate Width, b	Plate Moment of Inertia, I	Turret Mass, M_t	Turret Moment of Inertia, I_t	Young's Modulus for 7075-T651 Aluminum alloy, Y	Density for 7075-T651 Aluminum alloy, ρ
12.7 [mm]	254 [mm]	0.812 [kg·m^2]	1.511 [kg]	6.4 x 10^{-3} [kg/m^3]	71.7 [GPa]	2,810 [kg/m^3]

The oscillating turret assembly was tested in the 3' x 3' White Field tunnel at the University of Notre Dame. Figure 4, left, shows the turret attached to the oscillating plate. Figure 4, right, shows the schematic of the whole assembly, including a mounting cylindrical canister. The canister is used to attach the turret assembly to the tunnel wall, so only the hemisphere sticks into the flow.

The bottom of the hemisphere was aligned with the tunnel wall, with a small, about 1 mm, gap between the turret and the tunnel wall, shown in Figure 4, right, to guarantee the free motion of the turret in the spanwise direction. If the oscillating frequency coincides with the most energetic frequency of the shifting wake mode, $St_D = 0.15$, it is expected that the external forcing acting on the turret should amplify the natural periodic motion of the plate and turret assembly via resonance-related amplitude amplification, resulting in periodic single-frequency spanwise motion of the turret.

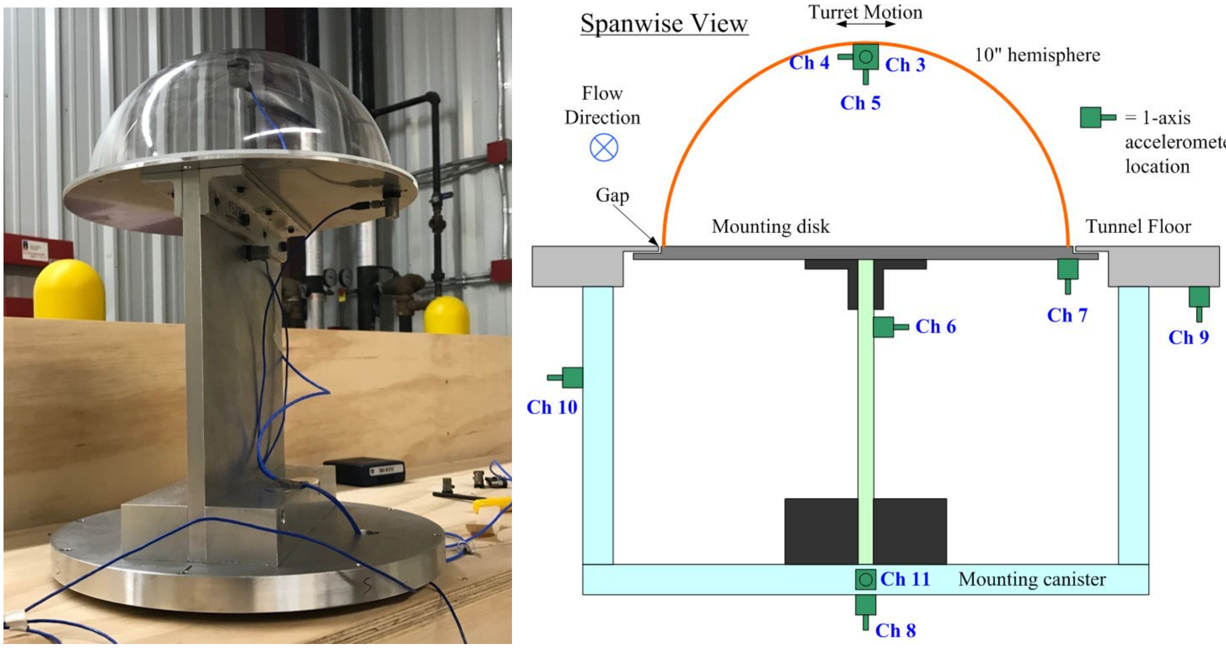

Figure 4: Left: A photograph of the turret assembly, without a mounting canister. Right. Schematic of the turret assembly along the spanwise direction and the locations of the 1-axis accelerometers. Measurement direction for each sensor is indicated by a small rectangle.

The oscillating turret system was also converted to a stationary turret configuration by removing metal spacers located underneath the back plate of the mounting canister, so the turret could be rigidly affixed and pressed against the tunnel wall. This configuration enabled two different sets of experiments to be conducted so the results of the oscillating turret could be compared to those of the same turret without the oscillations, a stationary turret case. A total of nine accelerometers were affixed to various locations inside of the turret and on the mounting plate and mounting canister, as shown in Figure 4, right. Accelerometer data was acquired simultaneously at 10 kHz for 30 seconds at incoming Mach numbers, $M = 0.30$, 0.35, 0.40, 0.45, 0.50, and 0.55 for the stationary turret and at $M = 0.30$, 0.35, 0.40, 0.45 for the oscillating turret. A summary of each test is presented in Table 2.

In order to study the wake response downstream of the turret, 11 unsteady differential Kulite pressure transducers were mounted flush on the tunnel wall downstream of the turret in the wake region. The unsteady pressure sensors were placed one turret diameter behind the oscillating turret assembly along the spanwise direction and spaced one inch apart. Figure 5 shows a cartoon representation of the positions of the pressure transducers in relation to the turret position, where

2R is the streamwise distance from the center of the turret to the streamwise location of the row of pressure transducers, *R* = 127 mm is the turret radius, and *z* designates the spanwise location of each transducer relative to *R*. Pressure data was collected at 10 kHz for 30 s simultaneously along with accelerometer data so that the wake dynamics behind the oscillating turret could be studied and compared to the wake dynamics of the fixed turret.

Table 2: Test parameters for each turret configuration.

Turret Configuration:	Incoming Mach Numbers:	Accelerometer Sampling Frequency:	Kulite Sampling Frequency:
Oscillating	M = 0.30, 0.35, 0.40, 0.45	3 kHz	30 kHz
Stationary	M = 0.30, 0.35, 0.40, 0.45, 0.50, 0.55	3 kHz	30 kHz

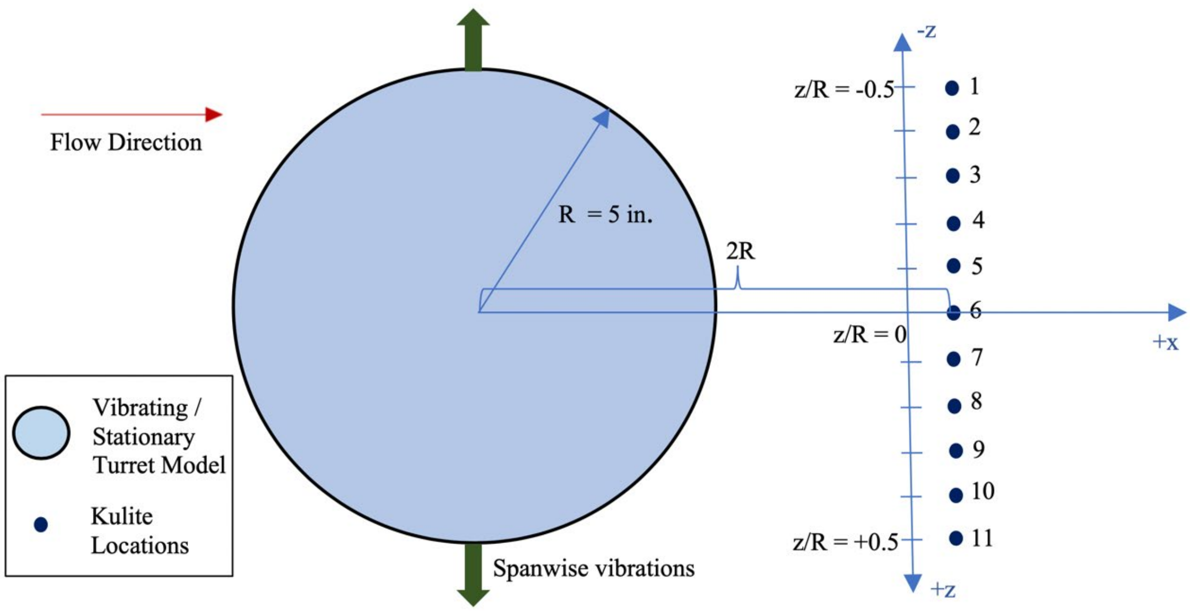

Figure 5: Schematic of the relative positions of the Kulite differential unsteady pressure sensors with respect to the oscillating/stationary turret.

The purpose of initial tests was to experimentally verify that the turret moves solely in the spanwise direction at a single frequency predicted by the linear cantilever bar theory and also measure the amplitude of the oscillations. Once these initial objectives were established, the primary purpose of the presented studies was to determine if the wake dynamics are modified when the turret oscillates at the dominant characteristic frequency of the wake.

III. Results

The power spectral density of the accelerometer at Channel 4, located at the top of the turret and oriented along the spanwise direction, see Figure 4, for both the stationary and the oscillating turrets for M = 0.5 are presented in Figure 6, along with the power spectral densities of the accelerometer at Channel 9, which measured the vibrations of the tunnel walls, indicated in Figure 4. While the Channel 4 spectrum for the stationary turret at this Mach number shows a broad range of excited frequencies, the spectra for the oscillating turret revealed the presence of a single strong dominant frequency at 87 Hz. This frequency is very close to the designed oscillating frequency of 90 Hz. Also, the amplitude of the dominant peak is more than 50 times larger than the largest peaks for the stationary turret. In addition to the dominant peak, a first harmonic with a smaller amplitude is also present in the signal for the oscillating turret, indicating some level of non-linear effects in the turret response. Since the tunnel was observed to oscillate substantially during the tests, the amplitude spectra from accelerometer Channel 9, which recorded the oscillations of the tunnel wall on which the turret assembly was mounted, are also shown in Figure 6. It is evident that the stationary turret spectra blend in well with the wall spectra and deviate significantly from the oscillating turret spectra in the frequency range corresponding to the highest levels of vibrational energy of the oscillating turret.

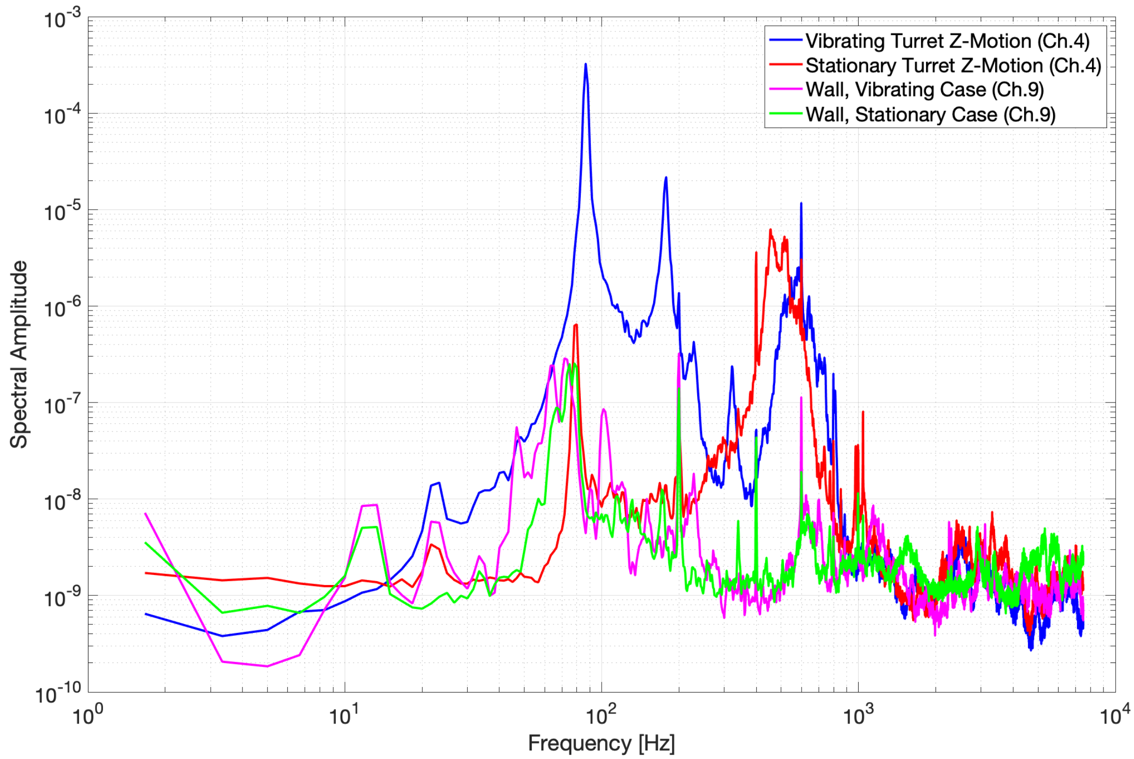

Figure 6: Power spectral density of accelerometer Ch.4 (turret spanwise motion) and Ch. 9 (wall motion) for both the oscillating and stationary turret configurations at M = 0.45.

To verify these findings, the normalized cross-spectral correlation was computed between the spanwise motion of the turret (Channel 4 in Figure 4) and wall vibrations (Channel 9 in Figure

4) for both oscillating and stationary cases, and the results are shown in Figure 7. The correlation amplitudes of the stationary turret and wall are noticeably higher than the correlation amplitudes of the oscillating turret and wall over the range of frequencies corresponding to where most of the energy of the oscillating turret was contained. The difference in correlation amplitudes are indicative that the oscillating turret was less physically coupled with the wall relative to the stationary case. Additionally, as Table 2 shows, approximately 62 percent of the oscillating turret motion occurred in the spanwise (z) direction, in comparison to 13 percent of the motion in the streamwise (x) and 25 percent of the motion in the cross-stream (y) directions. These percentages were computed by dividing the peak spectral amplitude of the oscillating turret by the peak spectral amplitude of the stationary turret for each of the three degrees of freedom. Table 3 also shows that similar results were obtained from the accelerometers which measured the x, y, and z motion on the turret itself along with accelerometers instrumented on the outside of the mounting canister, with the exception of a juxtaposition of x and y motion between the oscillating turret and the mounting canister. Thus, the results of the accelerometer measurements revealed that the free turret oscillates primarily at the resonant frequency predicted by Euler-Bernoulli beam theory with the spanwise amplitude much larger than for the stationary turret, and the oscillations of the free turret are mostly confined to the spanwise direction.

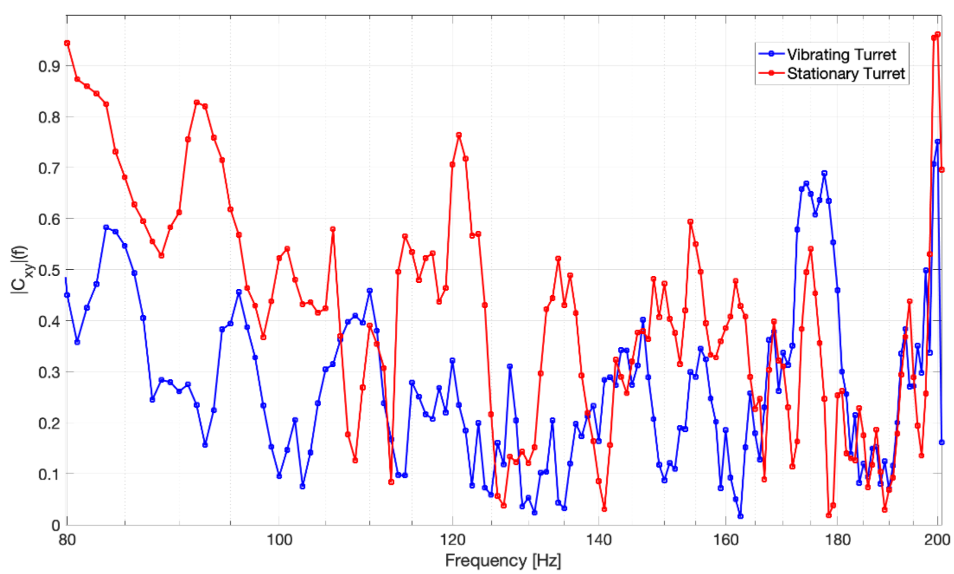

Figure 7: Normalized cross-spectral correlations between the spanwise turret motion (Ch. 4) and the tunnel wall vibrations (Ch.9) for oscillating and stationary cases at M = 0.45.

Spectra for the oscillating turret at other Mach numbers, shown in Figure 8, also revealed the presence of the dominant peak over a wide range of tested Mach numbers. The frequency of the dominant peak is not affected by the incoming speed, further confirming that this peak is related to the elastic properties of the turret assembly. The amplitude of the dominant peak as a function of Mach number is plotted in Figure 9. The amplitude increases with the Mach number increased, until it reaches a maximum value at M = 0.50. This is an expected behavior, as the unsteady forcing amplitude increases with the increased dynamic pressure. At a higher Mach number of 0.55, the amplitude starts decreasing. The drop-off at the highest Mach number can be attributed to the fact that the range of frequencies of the unsteady forcing also increases with the Mach number. Thus, while overall unsteady forcing is larger at M = 0.55, compared to M = 0.50, most of this forcing is shifted to higher frequencies, providing less external forcing at the fixed frequency of 87 Hz.

Table 3: Spectral peak amplitude ratio between the oscillating and stationary turrets for the x, y, and z motion measured on the oscillating turret itself and on the mounting canister exterior along with the total percentage of motion in each direction.

Turret Motion		Mounting Canister Motion	
x-motion (Ch.3)	5.367, (13.3%)	x-motion (Ch.10)	2.389, (26.5%)
y-motion (Ch.5)	10.16, (25.1%)	y-motion (Ch.8)	1.467, (16.3%)
z-motion (Ch.4)	24.97, (61.7%)	z-motion (Ch.11)	5.164, (57.3%)

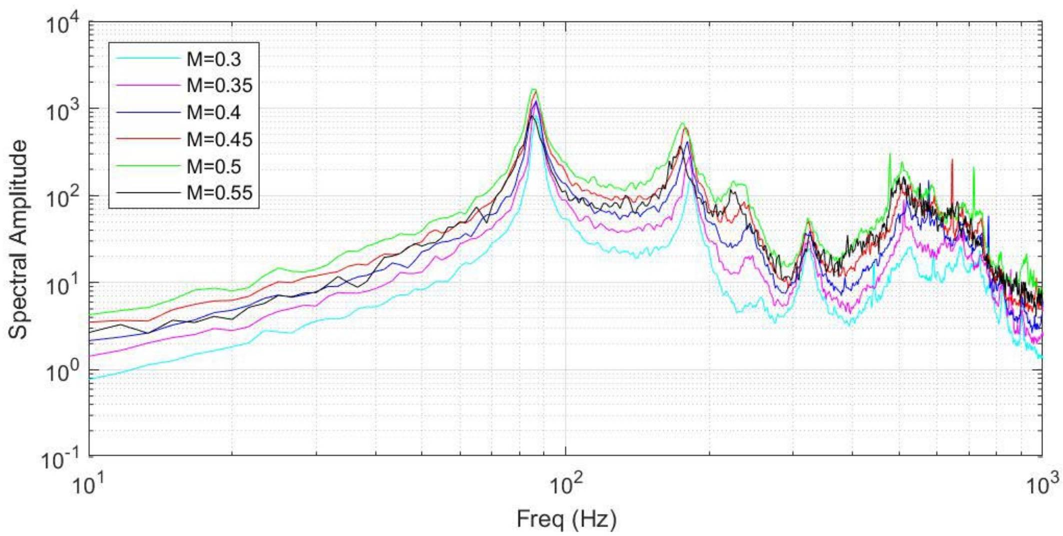

Figure 8: Accelerometer amplitude spectra of spanwise motion for the oscillating turret for a range of incoming Mach numbers.

The accelerometer data were high-pass filtered above 10 Hz and integrated in time twice to compute time series of the actual turret displacement. The results of the oscillating turret for M = 0.5 are given in Figure 10. The displacement time series show intermittent bursts of a single-frequency periodic motion, with the amplitude of approximately 0.5 mm. The burst durations are on the order of 0.2-0.3 seconds, or 15-25 periods of oscillations.

The similar analysis was also performed using the stationary turret data, and the representative results are shown in Figure 11. The turret motion for the stationary turret is much smaller in amplitude, about 0.1 mm, and at low ~10 Hz frequency. This motion is most probably related to the overall motion of the tunnel test section.

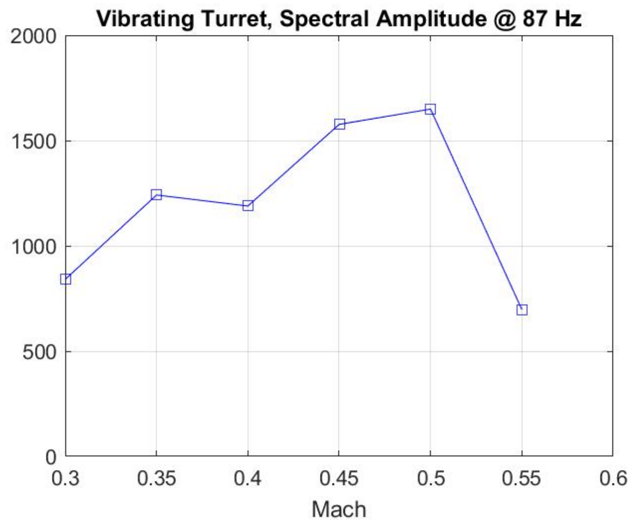

Figure 9: Amplitudes of the spectrum of the main oscillation peak for Accelerometer at Channel 4 for different incoming Mach numbers.

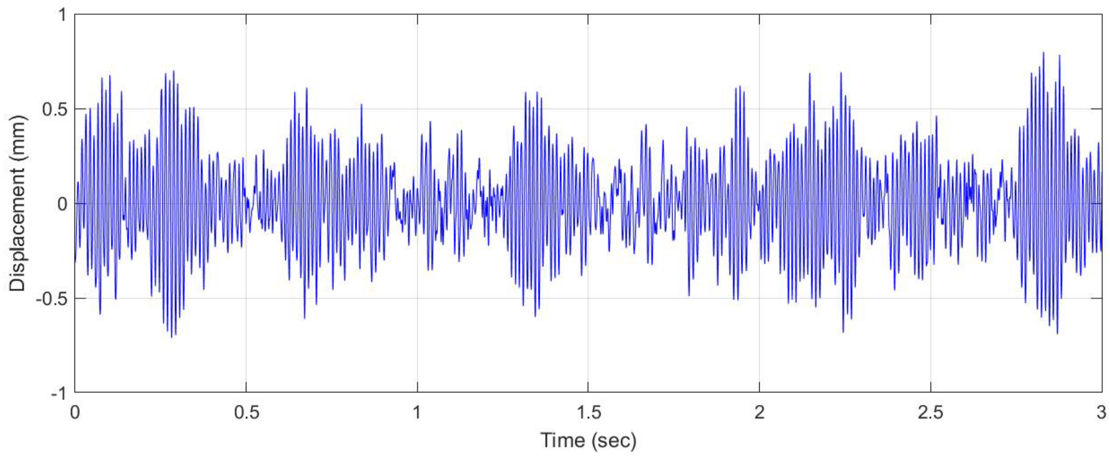

Figure 10: Turret displacement in the spanwise direction for the oscillating turret, reconstructed using accelerometer data from Channel 4 at M = 0.5.

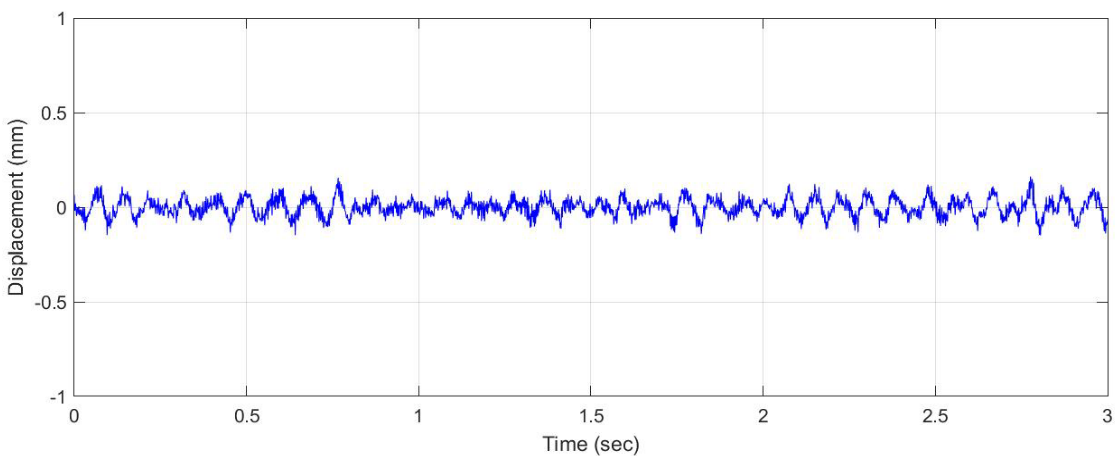

Figure 11: Turret displacement in the spanwise direction for the stationary turret, reconstructed using accelerometer data from Channel 4 at M = 0.5.

The rms pressure coefficient distributions for the oscillating and stationary cases are presented in Figure 12 for each tested Mach number. Both sets of distributions are substantially antisymmetric across the wake, especially more so for the oscillating case, which indicates that the presence of spanwise turret oscillations modify the pressure distribution in the wake by accentuating the wake shifting modality. However, the magnitudes of the maximum rms pressure coefficients at the same Mach numbers are very similar for both oscillating and stationary cases, which suggests that the oscillating turret wake does not contain more pressure energy under the same freestream conditions than the pressure energy contained in the stationary turret wake.

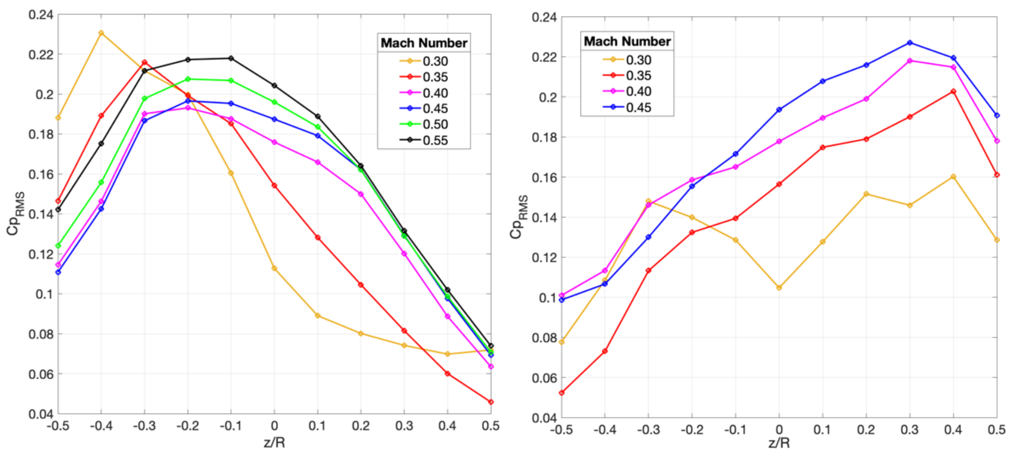

Figure 12: RMS pressure coefficient distributions in the wake for the fixed turret (left) and the oscillating turret (right).

To further investigate this behavior, pressure spectra from the unsteady pressure transducers in the wake were computed and compared for both turret configurations. The pressure spectra for the Kulite located at the middle of the wake for both turret configurations, where the RMS pressure coefficient values are approximately equivalent, are presented in Figure 13. The spectral amplitude of the unsteady pressure for the oscillating case was found to be noticeably lower across nearly the entire band of sampling frequencies at nearly all sampled wake positions, compared to the stationary turret case. It is an expected behavior, as a part of the incoming flow energy is transferred to an oscillating turret motion, and resulting in less energetic wake. Thus, the wake downstream of the oscillating turret is modified and contains less pressure "energy" than the stationary case.

Using the maximum rms pressure coefficient as a reference point for the highest comparable Mach number, M = 0.45, the normalized cross-spectral correlations were computed between the location where the rms pressure coefficient was maximum and all other unsteady pressure sensor locations for both cases. The results, given below in Figure 14, show the expected behavior of decreasing correlation amplitude with increased spacing between unsteady pressure sensors. However, a noticeable difference between the correlation for the oscillating turret and the stationary turret cases is the presence of a sharp increase in correlation amplitude in all of the oscillating turret correlations at 93 Hz that is not present in any of the stationary turret correlations. The frequency of these peaks is quite close (~7%) to the 87 Hz resonant frequency of the oscillating turret observed in the accelerometer spectra.

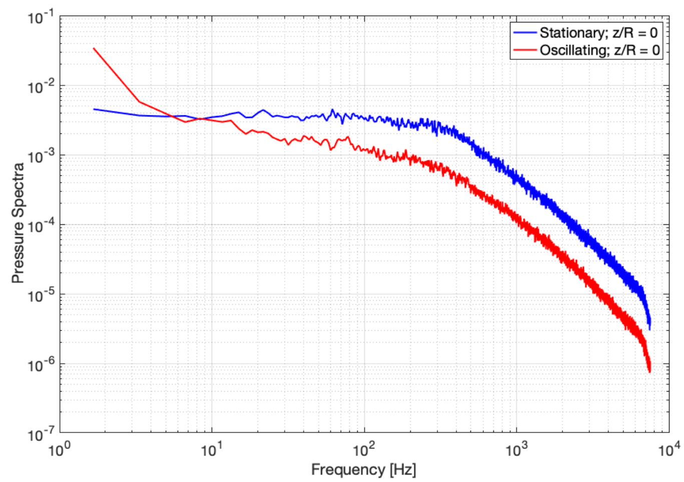

Figure 13: Pressure spectra from the middle of the wake (z/r = 0) for the oscillating and stationary turret configurations at M = 0.45.

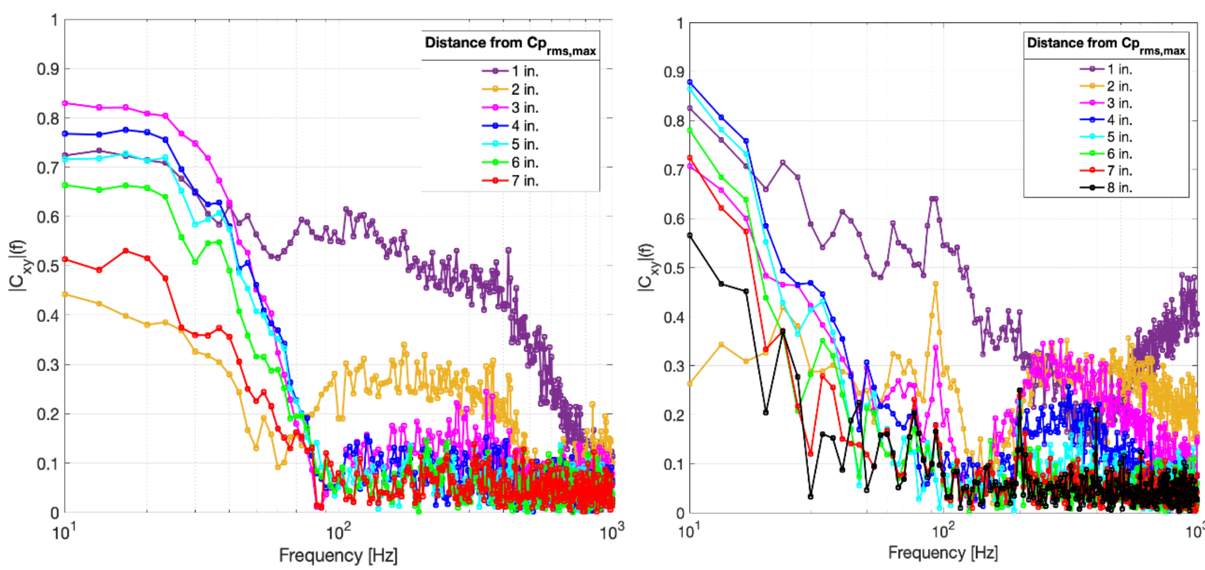

Figure 14: Normalized cross-spectral correlations between pressure data at the location where the rms pressure coefficient was maximum and other unsteady pressure sensor locations of increasing spacing for the stationary turret (left) and the oscillating turret (right), at M = 0.45.

Additional correlations between the unsteady pressure data and the wall motion recorded by an accelerometer confirmed that the increase in correlation amplitude was not an effect of contamination due to wall motion. The correlation amplitudes at the 93 Hz peak frequency along with the correlation amplitudes at the 87 Hz oscillating turret resonant frequency were plotted as a function of unsteady pressure sensor spacing, as given in Figure 15. The correlation amplitudes of the oscillating cases were higher than the correlation amplitudes of the stationary cases for both given frequencies over nearly all of the 1-8 in. range of unsteady pressure sensor spacing. This result implies that the presence of spanwise vibrations of the oscillating turret has an organizing effect on the wake dynamics at the resonant frequency of the oscillations in comparison to the stationary turret.

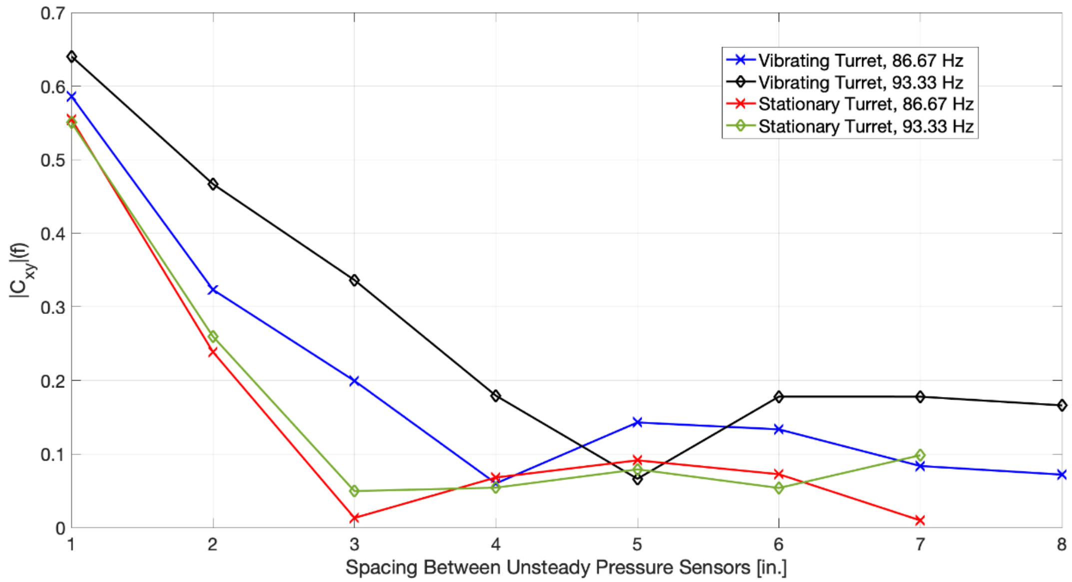

Figure 15: Normalized cross-spectral correlation amplitudes vs. unsteady pressure sensor spacing for the oscillating and stationary cases at the 87 Hz resonant frequency and also at the 93 Hz peak correlation amplitude.

IV. Conclusions

In the presented studies, the oscillating turret assembly has been designed, build and experimentally tested in a subsonic tunnel over a range of Mach numbers between 0.3 and 0.55. The hemispherical turret is mounted on a thin aluminum beam, allowing the turret to freely move in the spanwise direction only. Only the hemispheric turret was inserted into the flow. The oscillating turret was designed using Euler-Bernoulli beam theory to oscillate at a predominantly single resonant frequency. The parameters of the mounting beam were tuned for the oscillating frequency to coincide with the wake-dominant frequency of $St_D = 0.15$, so the resonant-based aero-elastic interaction would result in the forced turret oscillations. Turret-mounted accelerometer measurements demonstrated that the oscillations were indeed confined to the spanwise direction only. Normalized cross-spectral correlations between the spanwise motion and the wall vibrations showed a substantially lower correlation amplitude for the oscillating turret compared to the stationary case, eliminating all extraneous motion induced by the tunnel. Unsteady pressure sensors were placed in the spanwise direction one turret diameter from the turret center. Unsteady pressure data obtained simultaneously along with accelerometer data in the wake downstream of both the oscillating and stationary turrets revealed an antisymmetric pressure field along the spanwise extent of the wake, particularly for the oscillating turret configuration.

Using the wake locations in which unsteady pressure data yielded the highest rms pressure coefficient values as reference points, the normalized cross-spectral correlations of pressure data between the reference points and unsteady pressure sensor locations at an increasing distance from the reference locations yielded a higher correlation amplitude at the resonant frequency of the oscillating turret compared to the stationary turret over a wide range of sensor separations. The results of the pressure measurements indicate that the wake is more organized when the flow forces the turret to oscillate at the dominant frequency of the wake shifting mode. In addition, the pressure coefficient distributions indicate that the wake is less energetic for the oscillating turret configuration, and unsteady pressure spectra suggests that there is actually less energy contained in the oscillating turret wake compared to the stationary turret configuration. These findings are being currently further investigated in a follow-up study using pressure-sensitive paint to investigate the global pressure fields on and around both oscillating and stationary turrets.

Acknowledgements

This work is supported by the Air Force Research Laboratory, Cooperative Agreement number FA9451-17-2-0088. The U.S. Government is authorized to reproduce and distribute reprints for governmental purposes notwithstanding any copyright notation thereon.

References

[1] S. Gordeyev and E. Jumper, "Fluid Dynamics and Aero-Optics of Turrets", Progress in Aerospace Sciences, 46, (2010), pp. 388-400.

[2] B. Vukasinovic, A. Glezer, S Gordeyev, E. Jumper and W. W. Bower, "Flow Control for Aero-Optics Application", Experiments in Fluids, 54, p. 1492, 2013.

[3] N. De Lucca, S. Gordeyev and E.J. Jumper, "In-flight aero-optics of turrets", Journal of Optical Engineering, 52(7), 071405, 2013.

[4] C. Porter, S. Gordeyev, M. Zenk and E. Jumper, "Flight Measurements of the Aero-Optical Environment around a Flat-Windowed Turret", AIAA Journal, Vol. 51, No. 6, Jun. 2013, pp. 1394-1403.

[5] J. Morrida, S. Gordeyev, N. De Lucca, E.J. Jumper, " Shock-Related Effects on Aero-Optical Environment for Hemisphere-On-Cylinder Turrets at Transonic Speeds ", Applied Optics, 56(16), pp. 4814-4824, 2017.

[6] E. Mathews, K. Wang, M. Wang and E. Jumper, “LES of an Aero-Optical Turret Flow at High Reynolds Number”, AIAA 2016-1461, 2016.

[7] R. Jelic, S. Sherer and R.Greendyke, “Simulation of Various Turret Configurations at Subsonic and Transonic Flight Conditions Using OVERFLOW”, Journal of Aircraft, 50, pp. 398-409, 2013.

[8] Coirier, W.J, Porter, C., Barber, J., Stutts, J., Whiteley, M., Goorskey, D. and Drye, R.,”AeroOptical

[9] Evaluation of Notional Turrets in Subsonic, Transonic and Supersonic Regimes,” AIAA Paper 2014-2355, 2014

[10] P.E. Morgan and M.R. Visbal, “Hybrid Reynolds-Averaged Navier–Stokes/Large-Eddy Simulation Investigating Control of Flow over a Turret,” Journal of Aircraft, Vol. 49, No. 6, pp. 1700-1717, 2012.

[11] Ladd, J., Mani, A. and Bower, W., “Validation of Aerodynamic and Optical Computations for the Unsteady Flow Field About a Hemisphere-on-Cylinder Turret,” AIAA Paper 2009-4118, 2009.

[12] S. Gordeyev, N. De Lucca, E. Jumper, K. Hird, T.J. Juliano, J.W. Gregory, J. Thordahl and D.J. Wittich, " Comparison of Unsteady Pressure Fields on Turrets with Different Surface Features using Pressure Sensitive Paint ", Experiments in Fluids, 55, p. 1661, 2014.
[13] S. Gordeyev, N. De Lucca, J. Morrida, E.J. Jumper, and D.J. Wittich, " Conditional Studies of the Wake Dynamics of Hemispherical Turret Using PSP ", AIAA SciTech Forum, 8 - 12 Jan 2018, Kissimmee, FL, AIAA Paper 2018-2048.
[14] N. De Lucca, S. Gordeyev, J. Morrida, E.J. Jumper, and D.J. Wittich, " Modal Analysis of the Surface Pressure Field Around a Hemispherical Turret using Pressure Sensitive Paint ", AIAA Paper 2018-0932, 2018.
[15] S. Gordeyev, N. De Lucca, J. Morrida, E.J. Jumper, and D.J. Wittich, " Conditional Studies of the Wake Dynamics of Hemispherical Turret Using PSP ", AIAA Paper 2018-2048, 2018.
[16] N. De Lucca, S. Gordeyev, E. Jumper, K. Hird, T.J. Juliano, J.W. Gregory, J. Thordahl and D.J. Wittich, " The Estimation of the Unsteady Aerodynamic Force Applied to a Turret in Flight ", 44nd AIAA Plasmadynamics and Lasers Conference, 24-27 June 2013, San Diego, California, AIAA Paper 2013-3136.
[17] A. Erturk and D.J. Inman, *Piezoelectric Energy Harvesting*, 1st Edition, John Wiley & Sons, Ltd, 2011.